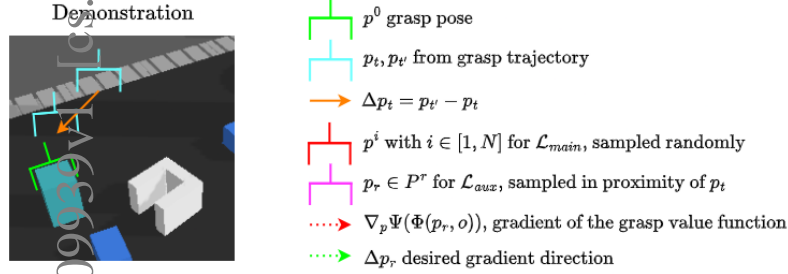


# Graphical Abstract

## dGrasp: NeRF-Informed Implicit Grasp Policies with Supervised Optimization Slopes

Gergely Soti, Xi Huang, Christian Wurrll, Björn Hein

We improve the training process of a grasp value function used in an implicit policy by employing an auxiliary loss function to supervise the gradients of the neural network by the trajectory.



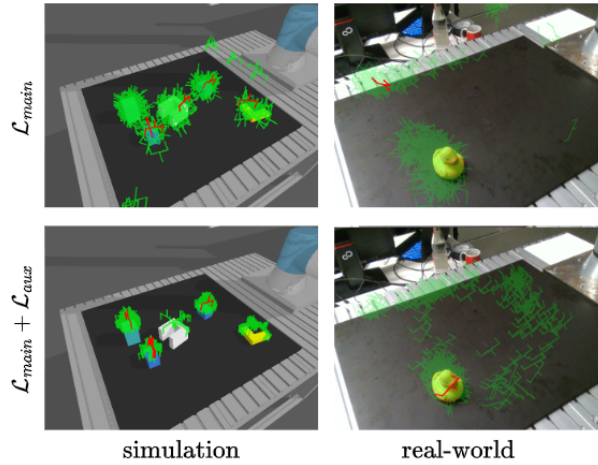
Main loss:

$$\mathcal{L}_{main} = -\log \frac{e^{\Psi(\Phi(p^0, o))}}{\sum_{i=0}^N e^{\Psi(\Phi(p^i, o))}}$$

Auxiliary loss:

$$\mathcal{L}_{aux} = -S_C(\Delta p_t; \nabla_p \Psi(\Phi(p_t, o)))$$

This leads to more stable policy convergence and improved success rates in simulated and real-world settings, with zero-shot sim-to-real transfer.



## Highlights

### **dGrasp: NeRF-Informed Implicit Grasp Policies with Supervised Optimization Slopes**

Gergely Soti, Xi Huang, Christian Wurrll, Björn Hein

- The approach uses grasp trajectories to supervise the training of an implicit grasp value model via second-order gradients during weight update.
- With this, more stable implicit grasp policies are achieved.
- This results in an improved performance in simulation and an improved zero-shot transfer to the real-world.

# dGrasp: NeRF-Informed Implicit Grasp Policies with Supervised Optimization Slopes

Gergely Soti<sup>a,b</sup>, Xi Huang<sup>b</sup>, Christian Wurrll<sup>a</sup>, Björn Hein<sup>a,b</sup>

<sup>a</sup>*Karlsruhe University of Applied Sciences, Institute of Robotics and Autonomous Systems, Karlsruhe, 76133, Germany*

<sup>b</sup>*Karlsruhe Institute of Technology, Institute of Anthropomatics and Robotics, Karlsruhe, 76131, Germany*

---

## Abstract

We present dGrasp, an implicit grasp policy with an enhanced optimization landscape. This landscape is defined by a NeRF-informed grasp value function. The neural network representing this function is trained on grasp demonstrations. During training, we use an auxiliary loss to guide not only the weight updates of this network but also the update how the slope of the optimization landscape changes. This loss is computed on the demonstrated grasp trajectory and the gradients of the landscape. With second order optimization, we incorporate valuable information from the trajectory as well as facilitate the optimization process of the implicit policy. Experiments demonstrate that employing this auxiliary loss improves policies' performance in simulation as well as their zero-shot transfer to the real-world.

*Keywords:* implicit policy, grasping, implicit representation, sim-to-real

---

## 1. Introduction

Robotic grasping is a fundamental task in the automation of object manipulation tasks. Despite extensive research and progress, dealing with unknown objects under real-world conditions is still a major challenge.

A recent and promising approach in this field is the concept of an implicit policy based on a learned value function. This function is optimized to identify optimal actions, which, in the context of grasping, translates to successful grasps. Building upon the implicit policy informed by a Neural Radiance Field (NeRF), originally developed in Soti et al. (2024), we propose to extend the learning process of the grasp value function in such a way that

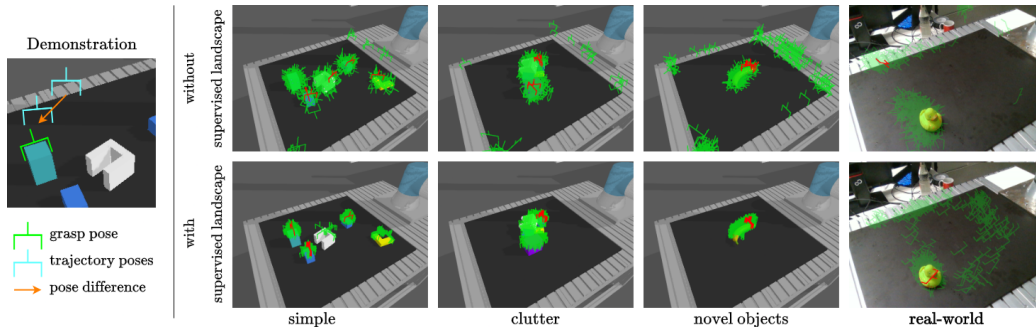


Figure 1: We incorporate the trajectory of the grasp demonstration into training the grasp value model to improve the convergence of the implicit policy. Supervising the optimization landscape of the policy this way leads to more stable convergence in the simulated and real-world tasks. The figure shows poses from a grasp demonstration on the left, and the final state of the policies optimization process on different tasks on the right. Policies employing a model with supervised optimization landscapes are shown in the bottom row. The best predicted grasp candidates are highlighted in red.

the slopes of the resulting optimization landscape would more effectively guide the optimization process to optimal grasp poses.

In an ideal optimization landscape, a successful grasp demonstration would move along the steepest slopes. In this work we want to encourage the optimization landscape during training to generate slopes that align with the demonstrated grasp trajectories. We do this by comparing the trajectory to the gradients of the landscape and minimizing the difference.

In essence, our approach aims to transform the challenge itself: instead of trying to climb a difficult mountain, we rather reshape the mountain to be easier to climb.

Our experiments, both in simulated and real-world settings, indicate that this approach of incorporating second-order optimization during training leads to more reliable and stable policy convergence.

While the principles presented here are not limited to grasping, this paper focuses specifically on their application within the context of robotic grasping.

The remainder of this paper is structured as follows: We begin with an overview of related work in the field, providing context and background for our research in Section 2. This is followed by a detailed description of our method in Section 3, where we outline the theoretical and practical aspects of our approach. We then present a series of experiments designed to evaluate our method in Section 4, along with a comprehensive analysis of the results

in Section 5. The paper concludes in Section 6 with a brief discussion of the findings, limitations of our work, and possible ideas for future research.

## 2. Related Work

Data-driven grasp synthesis for robotic object manipulation is a widely researched topic with a variety of approaches as detailed in the surveys by Bohg et al. (2013); Kleeberger et al. (2020); Newbury et al. (2023). Broadly, these methods fall into four categories: (i) object-detection based, (ii) reinforcement learning, (iii) supervised learning from a large, labeled dataset, and (iv) learning from demonstration.

In this work, we focus on behavior cloning, a popular end-to-end framework to learn policies from demonstrations, and even in behavior cloning there are two emerging branches, i.e. explicit and implicit models. Explicit models, like the works of Avigal et al. (2022); Florence et al. (2019); Rahmatizadeh et al. (2018); Zeng et al. (2020), propose actions directly from observations. Implicit models on the other hand learn to evaluate actions and are used in conjunction with sampling based or gradient-based optimization to find optimal actions (Florence et al. (2022); S3ti et al. (2024)). In this paper, we aim to extend the training process of such implicit models in a way that facilitates the optimization process, and thus improves the policy. In the following we review related work in the context of implicit policies and finally we discuss the core idea of our proposed approach.

Florence et al. (2022) investigated the effects of using implicit models for behavior cloning (IBC) across a variety of robot policy learning tasks. Their research highlights the distinct advantages of implicit models over explicit ones. They define an implicit policy as the argmin of a continuous energy function, which is learned from demonstrations. This energy function is expected to assign lower energies to optimal actions like the demonstrations, and higher energies otherwise. To find minimum locations and thus optimal actions, they propose two sampling-based algorithms and a gradient-based algorithm.

With a similar framework, we could successfully learn 3 degree-of-freedom (DoF) grasps (S3ti et al. (2023) ) and later extended it to 6DoF grasps in S3ti et al. (2024). Unlike IBC, which minimizes an energy function, these methods maximizes a value function. The key distinction here is however, the use of gradient-based optimization with the Adam optimizer Kingma and Ba (2014) instead of the gradient-based Langevin sampling described in IBC.

An additional key characteristic of the approach is the usage of a pre-trained neural radiance field (NeRF) Mildenhall et al. (2020); Lin et al. (2023) to inform the implicit model and thus requiring only RGB observations during inference.

NeRFs themselves learn an implicit representation of the environment, and have been used in various works involving robotic grasping (Ichnowski et al. (2021); Kerr et al. (2022); Dai et al. (2023); Blukis et al. (2023)). However, these applications primarily leverage NeRFs for augmenting observations or as feature extractors for explicit policies, differing from the implicit optimization-based framework we use.

Although Neural Motion Fields, by Chen et al. (2022), do not employ learning from demonstration, they also use an implicit model to learn a grasp value function and to generate grasp trajectories. In this approach, training the grasp value function requires a curated set of ground truth grasp poses and their model requires a segmented point cloud as input. Trajectories are generated by optimizing the learned implicit value function via sampling-based model predictive control.

Related to implicit models, Weng et al. (2023) approach grasp synthesis by predicting the distance of an action candidate to the nearest successful grasp and minimize this distance to achieve successful grasps. By integrating this distance metric into CHOMP motion planning as an additional cost, the model can generate grasp trajectories. For training, this method also requires a large grasp dataset and the model processes a segmented point cloud as input.

Diffusion Policies by Chi et al. (2023), use a denoising neural network that captures the gradient of the reversed diffusion process. They achieve this by minimizing the difference of a diffused action from ground truth and a synthetic denoised action. Given a sequence of observations, the policy uses the gradient field iteratively to denoise a sequence of randomly sampled actions and finally execute them. While the diffusion policy learns the gradient field to update action sequences from noisy ones, the landscape of implicit models captures the slope from an arbitrary state towards an optimal action. This means, that the optimization process of an implicit policy itself results in an action sequence.

In this current approach, our goal is to improve the optimization landscape of the implicit grasp policy described in S3ti et al. (2024). In addition to learning from the grasp pose itself, we use second-order optimization to supervise the gradients of the optimization landscape using the demonstrated

grasp trajectory. Although, using a second-order optimization algorithm like BFGS algorithm (Fletcher (2000)) might prove beneficial for training, such algorithms usually involve the computation of the Hamiltonian and its inverse which can be expensive. Instead, we use the Adam optimizer for both training and to lead the pose along the landscape during optimization, consistent with Yen-Chen et al. (2021); S3ti et al. (2023); S3ti et al. (2024).

### 3. Method

In this work, we build on a previously developed grasp value function S3ti et al. (2024), which assigns a score to 6-DoF Tool Center Point (TCP) poses based on their likelihood of resulting in a successful grasp. By maximizing this function through gradient-based optimization, initial TCP poses are refined towards more successful grasping outcomes. Central to the method is the use of transfer learning applied to a pretrained, image-conditioned NeRF that is initially trained for novel view synthesis. This NeRF acts as a backbone, providing a geometric representation of scenes from which the grasp value model is derived.

In the following, we first describe the baseline model in 3.1 using the methodology mentioned above. We then discuss our proposed approach to improve the optimization landscape in 3.2 and the optimization process in 3.3 for this baseline model.

#### 3.1. Preliminaries

The core of our baseline, as defined in S3ti et al. (2024), lies in the grasp value function,  $\Psi$ , a neural network conditioned on RGB image observations  $o$ , which maps TCP poses  $p$  to scalar values. Higher scores by  $\Psi$  indicate a greater likelihood of successful grasping. The grasp policy,  $\pi$ , is formulated as follows:

$$\pi(o) = \operatorname{argmax}_p \Psi(\Phi(p, o)) \quad (1)$$

Here,  $\pi(o)$  represents the optimal TCP pose for grasping. The function  $\Psi$  evaluates the activations of the pre-trained NeRF  $\Phi$  for a given pose  $p$  and RGB observations  $o$ . It is trained on demonstrations, by transforming the learning process into a binary classification problem. To achieve this, each demonstrated grasp is labeled with 1 and randomly sampled poses within the workspace serve as negative examples, labeled with 0 (see Figure 2). The observations  $o$  are camera images of the scene before executing the grasp.

With this setup, the categorical cross-entropy loss function is used during training:

$$\mathcal{L}_{main} = -\log \frac{e^{\Psi(\Phi(p^0, o))}}{\sum_{i=0}^N e^{\Psi(\Phi(p^i, o))}} \quad (2)$$

Here,  $p^0$  is the successful demonstration and  $p^i$  with  $i \in [1, N]$  are the sampled negative examples. This way, the model is trained to assign higher scores to demonstrated poses compared to other poses within the workspace.

The optimization process adapts a set of initial, randomly sampled input poses. A pose consists of a 3d position vector and the quaternion representation of its orientation. First, the translations are optimized for 16 iterations, then the quaternions for 16 iterations, both adapted via an Adam optimizer. After each optimization step, the quaternions are normalized.

In the next parts of this section, we will propose our conceptual and implementation changes to this baseline model.

### 3.2. Optimization Landscape

The optimization landscape for the pose optimization is shaped by the loss function in equation 2. This only considers the executed grasp pose. However, the grasp pose demonstrations also include the robots motion towards them. We hypothesize that the inclusion of the grasp trajectories can significantly improve the training and application of grasp value models, especially in such a pose optimization based setting. To this end, we augment the grasp value function  $\Psi$  to have the following property:

$$p_{t'} = p_t + \nabla_p \Psi(\Phi(p_t, o)) \quad (3)$$

with  $p_t$  the TCP pose at timestep  $t$  and  $p_{t'}$  the pose at a later timestep  $t'$  during a demonstration. On one hand, this aligns with the gradient based optimization of the initial poses. On the other hand, given that we have access to ground truth trajectories from demonstrations, this gradient can be supervised by the displacement of the TCP pose along the trajectory during training as an auxiliary loss:

$$\mathcal{L}_{aux} = -S_C(\Delta p_t, \nabla_p \Psi(\Phi(p_t, o))) \quad (4)$$

with  $\Delta p_t = p_{t'} - p_t$  represents the differences between the translation and the orientation representation of the pose. The cosine similarity  $S_C$  is applied to these differences and their corresponding gradients. The reasoning behind



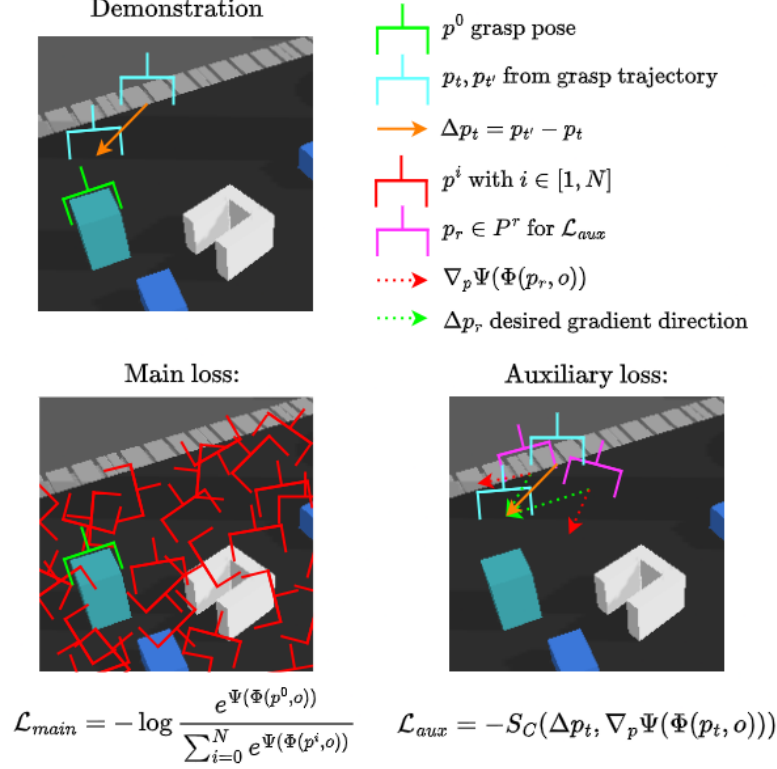


Figure 2: The main loss contributes to selecting the correct grasp (green) from the random generated ones (red). The Auxiliary loss enforces the gradients of the value function to be similar to the demonstrations.

cosine similarity is that we are mainly interested in the direction of the gradients. Since we use Adam to optimize the poses, instead of directly applying the gradients, we leave the smoothing and the control to the optimizer.

During training, we additionally augment the data from the grasp trajectory to compute the auxiliary loss. For a given observation  $o$ , current and future TCP poses  $p_t$  and  $p_{t'}$ , we sample a set of poses  $P^r$  in the proximity of  $p_t$ . The loss is then computed on  $\Delta p_r = p_{t'} - p_r$  and  $\nabla_p \Psi(\Phi(p_r, o))$  for each  $p_r \in P^r$ . We rationalize this decision with when a pose is near  $p_t$  then moving towards  $p_{t'}$  should still lead towards successful grasps. Figure 2 visualizes the differences between  $\mathcal{L}_{main}$  and  $\mathcal{L}_{aux}$ :  $\mathcal{L}_{main}$  aims at learning to identify good grasps and  $\mathcal{L}_{aux}$  learns how to get there.

Since we want to incorporate the gradient of  $\Psi$  into the loss function,

we need to consider the gradients of the error function  $S_C$  with respect to the weights  $\theta$  of  $\Psi$ , in particular because evaluating  $\Psi$  involves computing activations of the pre-trained NeRF  $\Phi$ :

$$\frac{dS_C}{d\theta} = \frac{dS_C}{d\frac{d\Psi}{dp}} \frac{d\frac{d\Psi}{dp}}{d\theta} = \frac{dS_C}{d\frac{d\Psi}{dp}} \frac{d(\frac{d\Psi}{d\Phi} \frac{d\Phi}{dp})}{d\theta} = \frac{dS_C}{d\frac{d\Psi}{dp}} \left( \frac{d\frac{d\Psi}{d\Phi}}{d\theta} \frac{d\Phi}{dp} + 0 \right) = \frac{dS_C}{d\frac{d\Psi}{dp}} \frac{d^2\Psi}{d\Phi d\theta} \frac{d\Phi}{dp} \quad (5)$$

$\Psi$  has a mixed partial derivative with respect to its weights  $\theta$  and the activations of  $\Phi$ . We have to avoid discontinuities in its first derivative, otherwise its second derivative could destabilize the weight update process. Since we are in the context of neural networks, we only have to make sure, that the derivative of activation function is continuous. In order to be able to use  $\mathcal{L}_{aux}$ , we swapped the the ReLU activation functions from the baseline method’s  $\Psi$  to ELU. As for the NeRF  $\Phi$ , it is sufficient to be differentiable with respect to the input TCP pose  $p$ . This means, that we still can use the pre-trained NeRF as it is.

The total loss for the model is then the sum of these two losses:

$$\mathcal{L}_{total} = \mathcal{L}_{main} + \mathcal{L}_{aux} \quad (6)$$

In our implementation of  $\mathcal{L}_{main}$  we use Keras’ built-in `KLDivergence` loss function instead of `CategoricalCrossentropy`. Although these two should yield equivalent results when applied in this one-hot encoded setting, using `KLDivergence` during our experiments required less computation time and even yielded better results.

### 3.3. Optimization Process

The optimization process relies on the Adam optimizer to adapt the input poses of  $\Psi$  in such a way that its output is maximized. This gradient-based pose optimization makes the selection of pose representation crucial. While the baseline method we investigate uses quaternions as the orientation representation, we now implement the 6D orientation representation proposed by Zhou et al. (2019), which has improved the performance of rotation processing neural networks on various tasks. For both orientation representations, however, we need to ensure that they are still valid orientations after the gradient-based update. In the case of quaternions we simply normalize the vector. In the case of the 6d representation being the first two column vectors of the rotation matrix, we follow the implementation of Zhou et al. (2019) where the adapted vectors are orthonormalized and the last column

is computed as their cross product. Additionally to this, when using  $\mathcal{L}_{aux}$ , the cosine similarity is computed for both predicted column vectors independently.

It is worth to note, that without the auxiliary loss, we can freely interchange pose representations, as they are only used during the optimization process and not during training. With the auxiliary loss however, the gradient used in equation 4 depends on the pose representation, thus for each representation a new model has to be trained.

We have also revised the optimization process. Instead of optimizing positions and rotations sequentially, we now optimize both simultaneously. This is particularly relevant when using the auxiliary loss, as it encourages simultaneous learning of gradients for both translations and rotations.

To tune the optimization process with the Adam optimizer we employ Bayesian hyperparameter optimization over 100 iterations. Hyperparameters include initial learning rates, decay rates, and the number of optimization steps. In case of sequential optimization, translations and rotations are optimized both for the given amount of steps. For synchronous optimization, both are optimized simultaneously for the number of optimization steps. For each other parameter — rotation representation, the application of the auxiliary loss, and optimization strategy — an independent tuning process is conducted. The model with the highest validation success, determined through grasp execution in simulation, is selected for testing.

## 4. Experiments

To evaluate the grasp policies, we conduct a series of experiments in both simulated and real-world environments. These experiments are designed to test the models’ ability to generalize across familiar (in-distribution) and unfamiliar (out-of-distribution) scenarios and their adaptability to real-world conditions.

We use the three simulated and a real-world task described in S3ti et al. (2024) to measure the grasp success rate of a policy:

- Tasks in a pybullet simulated environment. Grasping is successful if an object is enveloped by the gripper fingers and was lifted up after the physics-based grasp execution
  - **simple:** This task assesses basic grasping capabilities. The workspace contains up to five monochromatic prismatic objects, each placed

at a distance from the others. The goal is to successfully grasp one of these objects.

- **clutter:** This task tests the model’s performance on out-of-distribution pose data. The scenario is a cluttered workspace containing five monochromatic prismatic objects. The objective is to grasp all objects one after the other.
- **novel objects:** This task assesses the model’s ability to handle out-of-distribution pose, shape, and texture data. The workspace features one previously unseen object selected from the YCB dataset Calli et al. (2015). The goal is to grasp this object. Objects used: banana, foam brick, gelatin box, hammer, Master Chef can, pear, power drill, strawberry and tennis ball.
- **real-world:** This task tests the transferability of the model to the real world. In this task, a single everyday object is randomly placed in the workspace of an real robot. The task is considered successful if the robot can securely grasp and lift the object. Objects used: tennis ball, crochet ball, small Lego tire, large Lego tire, can of beans, rubber duck, hiking boot, power drill, shampoo bottle and a 3d printed block.

All tasks feature a UR10 robot on a workbench, equipped with a Robotiq 2f-140 gripper and an Intel RealSense D415 camera. Examples of these tasks are shown in Figure 3.

#### 4.1. Training

During training, all models were exclusively exposed to the training dataset of the simulated **simple** scenario, including the pre-training of the NeRF and the grasp value models. This means, that neither of the models have ever seen objects in close proximity, with complex textures and shapes or in poses other than upright during training.

Training data samples are generated in simulation, and contain RGB observations and the grasp trajectory. Successful grasp poses are determined by an oracle with access to the simulation’s state. When training only with the main loss  $\mathcal{L}_{main}$  we only use the final grasp pose for supervision. Only if  $\mathcal{L}_{aux}$  is also employed is the grasp trajectory used as well during training. The training data was generated over 512 randomly set up scenarios with the five objects successively removed, resulting in a total number of 2560 successful grasp demonstrations.

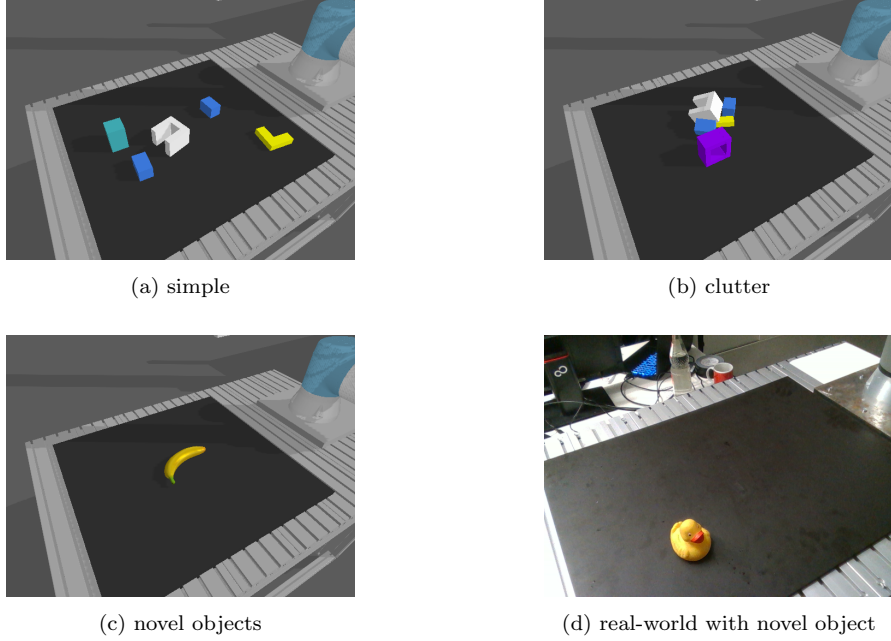


Figure 3: Example observations from the test datasets.

We only train one baseline model **Base**, since the rotation representation and the sequential or synchronous nature of the optimization is handled by the optimization process (see section 3.3). In case of using  $\mathcal{L}_{aux}$  we need to train two models, one with quaternions **dGrasp<sub>quat</sub>** and one with 6d rotation representation **dGrasp<sub>6d</sub>**.

#### 4.2. Hyperparameter tuning

The hyperparameter tuning of the optimization process is guided by grasp success rates on the validation data of the **simple** task, which does not include ground truth data. Only the observations are used, and the policy is executed in simulation to determine whether a proposed grasp was successful. The validation data consists of 10 randomly set up scenarios with 5 objects, and the robot is allowed to execute 5 grasp attempts, resulting in an overall of 50 grasp attempts. The hyperparameters tuned are described in 3.3.

From the **Base** and **dGrasp** models we can derive 8 policies via tuning the optimization parameters: **Base<sub>quat-seq</sub>**, **Base<sub>quat-sync</sub>**, **Base<sub>6d-seq</sub>**, **Base<sub>6d-sync</sub>**, **dGrasp<sub>quat-seq</sub>**, **dGrasp<sub>quat-sync</sub>**, **dGrasp<sub>6d-seq</sub>** and **dGrasp<sub>6d-sync</sub>**. These result from combining the different rotation representations with subscripts  $[\cdot]_{quat}$

and  $[\cdot]_{6d}$  and whether the position and the orientation should be optimized sequentially or synchronously with subscripts  $[\cdot]_{\text{seq}}$  and  $[\cdot]_{\text{sync}}$ . We consider  $\text{Base}_{\text{quat-seq}}$  to be our baseline, as it follows the model described in S3ti et al. (2024).

## 5. Results

In this section, we present the results of our experiments, and evaluate the performance of our obtained policies in both simulated and real-world environments. The emphasis is on assessing how our models perform on familiar data and their ability to generalize to unfamiliar data with variations in pose, texture, and shape. Additionally, we explore the zero-shot transfer capabilities of these models to real-world settings.

We compare the performance of our policies not only against our baseline  $\text{Base}_{\text{quat-seq}}$  but also against the reported results of the MV1 policy from S3ti et al. (2024),  $\text{Base}_{\text{reported}}$ . While both models have the same configuration with quaternions as rotation representation and sequential optimization process, due to computational resource constraints, we reduce the batch size during training of  $\Phi$  and  $\Psi$  from 8 to 4 for all of our models, including  $\text{Base}_{\text{quat-seq}}$ . However, during inference, it is possible to execute  $\Psi$  multiple times in parallel and apply the gradient-based optimization process to the combined results. Our setup is limited to using 2 images from different perspectives simultaneously, as opposed to 3 as described in S3ti et al. (2024). Additionally, the number of random initial poses during the optimization process is reduced from 8k to 4k. We trained our models on an NVIDIA RTX A4500 GPU.

With these comparisons we aim to gain clearer insights into the specific contributions of our proposed enhancements and the limitations imposed by reduced computational resources to the overall performance of our models.

### 5.1. Simulated Grasping

The test datasets of the simulated tasks only provide the observations to the policy. The grasp success is measured by executing the proposed grasps in simulation. The simple and clutter test datasets contain 10 randomly arranged scenarios of 5 objects, with an allowed number of 5 grasp attempts per scenario. The simple and clutter test datasets contain 10 randomly set up scenarios with 5 objects, with an allowed number of 5 grasp attempts per scenario. In the case of the novel objects task, the test dataset contains

Table 1: Grasp success rates in simulated tasks. **Base<sub>reported</sub>** contains the results reported in S3ti et al. (2024). Highlighted are the best of our and the overall best policies.

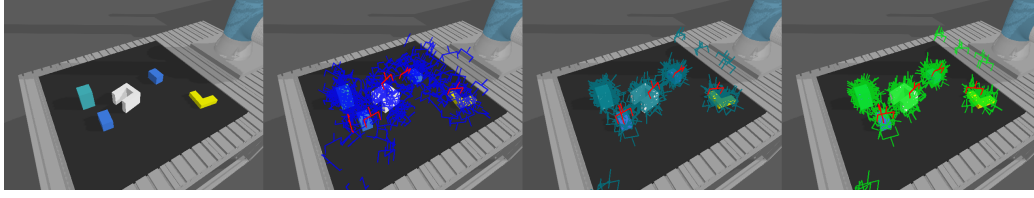
	simple	clutter	novel objects	average
<b>Base<sub>reported</sub></b>	0.88	0.58	<b>0.44</b>	0.633
<b>Base<sub>quat-seq</sub></b>	0.8	0.604	0.348	0.584
<b>Base<sub>quat-sync</sub></b>	0.796	0.756	0.384	0.645
<b>Base<sub>6d-seq</sub></b>	0.792	0.688	<b>0.424</b>	0.635
<b>Base<sub>6d-sync</sub></b>	0.784	0.692	0.36	0.612
<b>dGrasp<sub>quat-seq</sub></b>	0.94	0.72	0.316	0.659
<b>dGrasp<sub>quat-sync</sub></b>	<b>0.956</b>	0.748	0.332	0.679
<b>dGrasp<sub>6d-seq</sub></b>	0.944	<b>0.8</b>	0.32	<b>0.688</b>
<b>dGrasp<sub>6d-sync</sub></b>	0.912	0.756	0.28	0.649

50 scenarios with a random selected object. After optimizing the random generated initial poses, the one with the highest final value is selected for execution. This random initialization, makes the policies non-deterministic, so we run each simulated experiment 5 times and show the average success rates in Table 1, together with **Base<sub>reported</sub>**. In the following, we compare the performance of our policies in the three tasks.

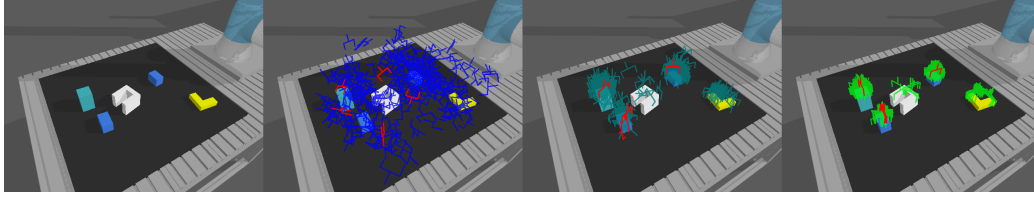
In the simple task, **Base<sub>reported</sub>** outperforms all of our **Base<sub>[.]</sub>** models. Our proposed modifications even slightly underperform compared to **Base<sub>quat-seq</sub>**. However, the application of auxiliary loss in our **dGrasp<sub>[.]</sub>** policies shows a significant improvement over **Base<sub>reported</sub>** and all our **Base<sub>[.]</sub>** models. Figure 4 also indicates a more stable convergence of the policy **dGrasp<sub>quat-sync</sub>** with the auxiliary loss applied.

In the clutter task, **Base<sub>quat-seq</sub>** performs slightly better, than **Base<sub>reported</sub>**. All our enhancements positively affect the success rate. Notably, the integration of auxiliary loss further improves the performance. Figure 5 shows the optimization process of the baseline policy **Base<sub>quat-seq</sub>** and **dGrasp<sub>6d-seq</sub>** with auxiliary loss.

In the novel objects task however, **Base<sub>reported</sub>** significantly outperforms all our policies. A plausible explanation is the increased difficulty in generalizing to novel objects, which present new challenges in terms of pose, shape, and color. The batch size during training likely plays a critical role here. For our **Base<sub>[.]</sub>** models, we had to reduce batch sizes, and for the **dGrasp<sub>[.]</sub>**

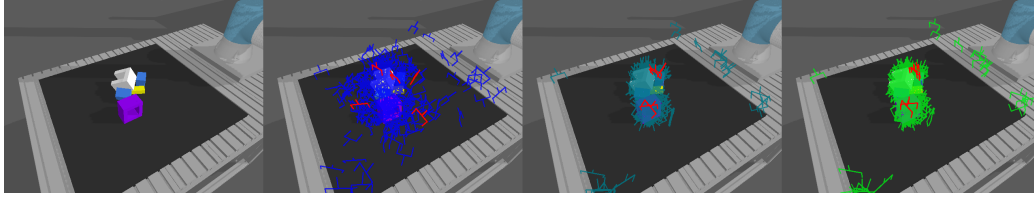


(a)  $\text{Base}_{\text{quat-seq}}$

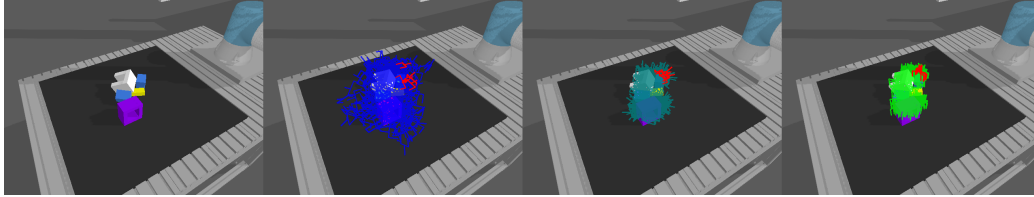


(b)  $\text{dGrasp}_{\text{quat-sync}}$

Figure 4: Policy optimization process of the baseline policy  $\text{Base}_{\text{quat-seq}}$  and the best performing policy  $\text{dGrasp}_{\text{quat-sync}}$  on the simple task. Shown are grasp candidates with highest final predicted values. The five trajectories with the highest values are highlighted in red. Starting from the blue initialization, the optimization shift the candidates along the gradients. The color from blue to green indicates the progress of optimization.



(a)  $\text{Base}_{\text{quat-seq}}$



(b)  $\text{dGrasp}_{6\text{d-seq}}$

Figure 5: Policy optimization process of the baseline policy  $\text{Base}_{\text{quat-seq}}$  and the best performing policy  $\text{dGrasp}_{6\text{d-seq}}$  on the clutter task. Shown are grasp candidates with highest final predicted values. The five trajectories with the highest values are highlighted in red. Starting from the blue initialization, the optimization shift the candidates along the gradients. The color from blue to green indicates the progress of optimization.



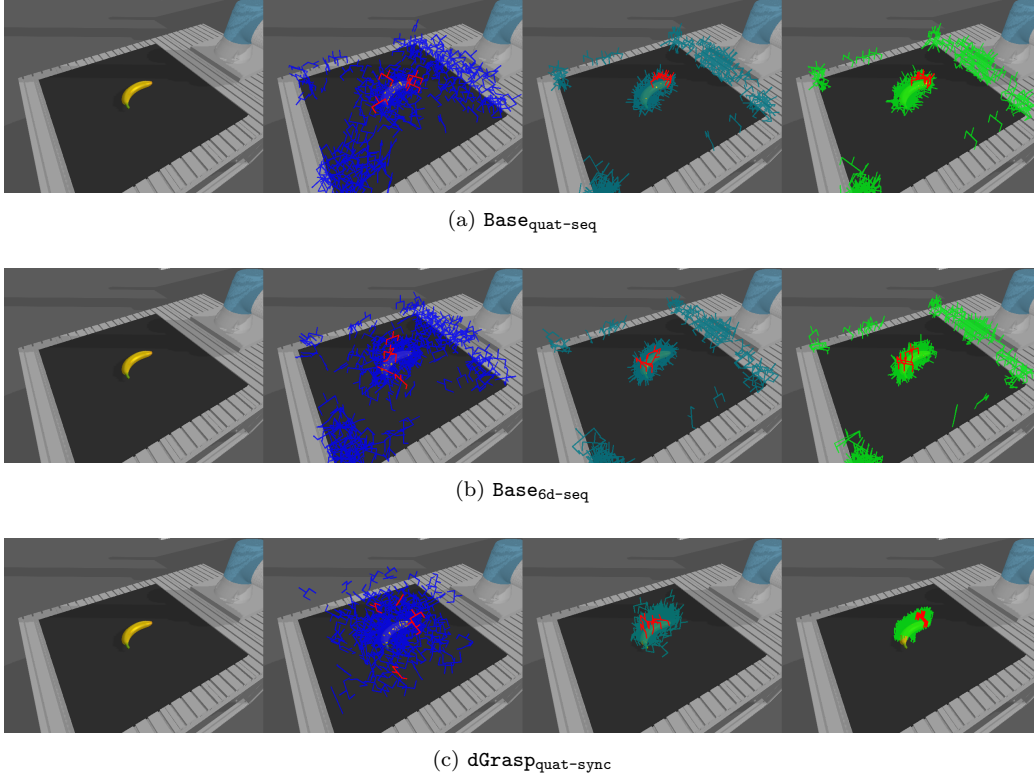


Figure 6: Policy optimization process of the baseline policy  $\text{Base}_{\text{quat-seq}}$ , the best performing policy  $\text{Base}_{6\text{d-seq}}$  and the best performing  $\text{dGrasp}_{[\cdot]}$  policy on the novel objects task. Shown are grasp candidates with highest final predicted values. The five trajectories with the highest values are highlighted in red. Starting from the blue initialization, the optimization shift the candidates along the gradients. The color from blue to green indicates the progress of optimization.

models, the number of poses used during training was significantly decreased from 512 to 64 due to the computational demands of processing second order gradients. This reduction may also explain to the lower performance of policies employing auxiliary loss.

Even though Figure 6 shows a more stable convergence of the  $\text{dGrasp}_{[\cdot]}$  policies, these often resulted in grasps slightly above the object. This was less the case for the  $\text{Base}_{[\cdot]}$  models trained only with the main loss. These however often converged to one of the corners of the workspace. Most policies were able to reliable grasp objects with simple shapes and textures: tennis ball, banana and pear, but struggled with other types of objects.

Table 2: Grasp success rates in the real-world. **Base<sub>reported</sub>** is the result reported in S3ti et al. (2024). Highlighted is the best of our and the overall best policy.

	real-world
<b>Base<sub>reported</sub></b>	<b>0.4</b>
Base <sub>quat-seq</sub>	0.08
Base <sub>quat-sync</sub>	0.08
Base <sub>6d-seq</sub>	0.1
Base <sub>6d-sync</sub>	0.14
dGrasp <sub>quat-seq</sub>	<b>0.32</b>
dGrasp <sub>quat-sync</sub>	0.3
dGrasp <sub>6d-seq</sub>	0.26
dGrasp <sub>6d-sync</sub>	0.28

Contrary to the expected advantage of synchronous optimization in combination with auxiliary loss, the results do not reflect such a behavior.

Nonetheless, the application of auxiliary loss shows a considerable improvement in performance for the simple and clutter tasks. Generalizing to more complex objects however, still poses a huge challenge. In this context, it is important to note that these findings are based on our setup, which utilized only 2 images and 4k random initial poses for optimization, but we believe, that the primary factor affecting the performance in the novel objects task was the constrained batch size during training.

### 5.2. Real-World Grasping

In the real-world tests, each object is presented to the robot 5 times, and only one grasp attempt is allowed for each presentation. The results are shown in Table 2, along with **Base<sub>reported</sub>** from S3ti et al. (2024). To reduce the challenges posed by real-world data, before selecting the pose with the highest value, we filter the final results to contain only poses that are pointing downwards, meaning, that the  $\cos$  of the pose’s  $z$  axis and the origin coordinate systems  $z$  axis is negative. Additionally, to somewhat compensate the errors in camera calibration, we adjusted the final pose along its  $z$  axis by 1cm.

None of the policies were able to grasp the Lego tires. All attempts consistently converged towards one of the corners of the robot’s workspace. This was, in fact, the most common type of failure for the **Base<sub>[.]</sub>** models. Another

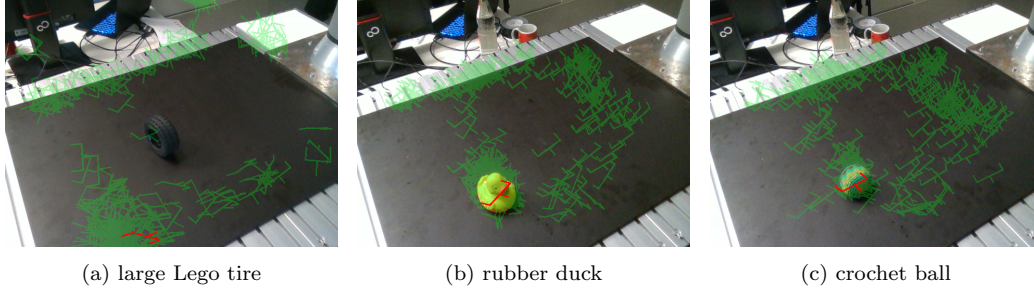


Figure 7: Figure (a) depicts a failure scenario where the optimization converges to the workspace corner. Figure (b) shows a common failure case of slippage. Figure (c) represents a successful grasp. The transparent poses indicate grasp candidates with the highest final predicted grasp values post-optimization, with the red pose representing the selected action.

frequent issue was the slight misalignment of the predicted grasp, either missing the object or causing a collision, particularly noticeable with the power drill, the can of beans, and the hiking boot. For grasping the rubber duck and shampoo bottle, a recurring failure case was slippage. Overall, the 3D printed block, tennis ball, and crochet ball were among the objects most consistently and successfully grasped, in particular by the **dGrasp<sub>[.]</sub>** models. Figure 7 illustrates various outcomes from our real-world testing, common failure scenarios and a successful grasps.

The performance of **Base<sub>quat-seq</sub>** in the real-world shows a noticeable decline compared to **Base<sub>reported</sub>**. This can partly be attributed to the same factors impacting performance in the simulated novel objects task (refer to Section 5.1), since the models have never seen real world objects. Additionally, a likely significant factor is the compounded error in camera calibration, which might have been more effectively mitigated with the third perspective employed with **Base<sub>reported</sub>**.

Despite these constraints, integrating auxiliary loss into our models significantly improved their performance. This is in contrast with our findings in the novel objects task, where **dGrasp<sub>[.]</sub>** models did not demonstrate the same level of effectiveness. In real-world scenarios, **dGrasp<sub>[.]</sub>** models notably outperformed the **Base<sub>[.]</sub>** models when handling simpler objects such as the 3D printed block, the crochet ball, and the shampoo bottle. However, both model types still faced challenges with more complex objects, indicating that the sim-to-real transfer of the policy, particularly with simpler objects, was significantly improved by using auxiliary loss.

Although `dGrasp` models do not reach the levels achieved by `Basereported`, the improvement they demonstrate highlights the efficacy of the auxiliary loss during training the grasp value function.

## 6. Conclusion

In this work, we proposed an auxiliary loss for augmenting the training of a NeRF-informed grasp value function. The goal of this auxiliary loss is to improve the optimization landscape of an implicit grasp policy. Through this loss, the demonstrated grasp trajectory supervises the gradients of the value function. Our approach shows significant improvements in two out of three simulated tasks and real world. Our results suggest that using this loss leads to a more stable convergence of the policy’s optimization process, thereby finding successful grasp poses more reliably. While exploring quaternions and a 6D representation for rotations and different optimization strategies (sequential and synchronous), we did not observe any definitive trends affecting performance.

Remarkably, our enhanced policies achieve comparable results to our reference work Soti et al. (2024), despite being significantly more limited in terms of computational resources. This demonstrates the efficacy of our approach in terms of generalization in simulation, and more importantly, in zero-shot transfer to real-world scenarios.

Nevertheless, the model’s generalization to novel objects remains a key challenge, which we believe could be mitigated by increasing computational resources. In addition, the model’s reliance on precise camera calibration presents another area for potential improvement.

Importantly, the proposed method is not restricted to grasping and can potentially be applied to a wide range of implicit policies. Although we implemented it in an open-loop context, our findings suggest the viability of transitioning to a closed-loop framework. This opens up the possibility of integrating the methods into more sophisticated tasks, such as trajectory generation, or into different learning frameworks such as learning from play data.

## Acknowledgement

This research is being conducted as part of the KI5GRob project funded by the German Federal Ministry of Education and Research (BMBF) under project number 13FH579KX9.

## Declaration of Generative AI and AI-assisted technologies in the writing process

Statement: During the preparation of this work the author(s) used ChatGPT in order to improve readability of the manuscript. After using this tool/service, the author(s) reviewed and edited the content as needed and take(s) full responsibility for the content of the publication.

## References

- Avigal, Y., Berscheid, L., Asfour, T., Kröger, T., Goldberg, K., 2022. Speedfolding: Learning efficient bimanual folding of garments, in: 2022 IEEE/RSJ International Conference on Intelligent Robots and Systems (IROS), IEEE. pp. 1–8.
- Blukis, V., Lee, T., Tremblay, J., Wen, B., Kweon, I.S., Yoon, K.J., Fox, D., Birchfield, S., 2023. One-shot neural fields for 3d object understanding. *arXiv:2210.12126*.
- Bohg, J., Morales, A., Asfour, T., Kragic, D., 2013. Data-driven grasp synthesis—a survey. *IEEE Transactions on robotics* 30, 289–309.
- Calli, B., Singh, A., Walsman, A., Srinivasa, S., Abbeel, P., Dollar, A.M., 2015. The ycb object and model set: Towards common benchmarks for manipulation research, in: 2015 international conference on advanced robotics (ICAR), IEEE. pp. 510–517.
- Chen, Y.C., Murali, A., Sundaralingam, B., Yang, W., Garg, A., Fox, D., 2022. Neural motion fields: Encoding grasp trajectories as implicit value functions. *arXiv preprint arXiv:2206.14854*.
- Chi, C., Feng, S., Du, Y., Xu, Z., Cousineau, E., Burchfiel, B., Song, S., 2023. Diffusion policy: Visuomotor policy learning via action diffusion. *arXiv preprint arXiv:2303.04137*.
- Dai, Q., Zhu, Y., Geng, Y., Ruan, C., Zhang, J., Wang, H., 2023. Grasp-nerf: multiview-based 6-dof grasp detection for transparent and specular objects using generalizable nerf, in: 2023 IEEE International Conference on Robotics and Automation (ICRA), IEEE. pp. 1757–1763.
- Fletcher, R., 2000. Practical methods of optimization. John Wiley & Sons.

- Florence, P., Lynch, C., Zeng, A., Ramirez, O.A., Wahid, A., Downs, L., Wong, A., Lee, J., Mordatch, I., Tompson, J., 2022. Implicit behavioral cloning, in: Conference on Robot Learning, PMLR. pp. 158–168.
- Florence, P., Manuelli, L., Tedrake, R., 2019. Self-supervised correspondence in visuomotor policy learning. *IEEE Robotics and Automation Letters* 5, 492–499.
- Ichnowski, J., Avigal, Y., Kerr, J., Goldberg, K., 2021. Dex-nerf: Using a neural radiance field to grasp transparent objects. *arXiv preprint arXiv:2110.14217* .
- Kerr, J., Fu, L., Huang, H., Avigal, Y., Tancik, M., Ichnowski, J., Kanazawa, A., Goldberg, K., 2022. Evo-nerf: Evolving nerf for sequential robot grasping of transparent objects, in: 6th Annual Conference on Robot Learning.
- Kingma, D.P., Ba, J., 2014. Adam: A method for stochastic optimization. *arXiv preprint arXiv:1412.6980* .
- Kleeberger, K., Bormann, R., Kraus, W., Huber, M.F., 2020. A survey on learning-based robotic grasping. *Current Robotics Reports* 1, 239–249.
- Lin, K.E., Lin, Y.C., Lai, W.S., Lin, T.Y., Shih, Y.C., Ramamoorthi, R., 2023. Vision transformer for nerf-based view synthesis from a single input image, in: Proceedings of the IEEE/CVF Winter Conference on Applications of Computer Vision, pp. 806–815.
- Mildenhall, B., Srinivasan, P.P., Tancik, M., Barron, J.T., Ramamoorthi, R., Ng, R., 2020. Nerf: Representing scenes as neural radiance fields for view synthesis, in: ECCV.
- Newbury, R., Gu, M., Chumbley, L., Mousavian, A., Eppner, C., Leitner, J., Bohg, J., Morales, A., Asfour, T., Kragic, D., et al., 2023. Deep learning approaches to grasp synthesis: A review. *IEEE Transactions on Robotics* .
- Rahmatizadeh, R., Abolghasemi, P., Bölöni, L., Levine, S., 2018. Vision-based multi-task manipulation for inexpensive robots using end-to-end learning from demonstration, in: 2018 IEEE international conference on robotics and automation (ICRA), IEEE. pp. 3758–3765.

- Sóti, G., Hein, B., Wurrll, C., 2023. Gradient based grasp pose optimization on a nerf that approximates grasp success, in: Intelligent Autonomous Systems 18, Springer.
- Sóti, G., Huang, X., Wurrll, C., Hein, B., 2024. 6-dof grasp pose evaluation and optimization via transfer learning from nerfs. [arXiv:2401.07935](#).
- Weng, T., Held, D., Meier, F., Mukadam, M., 2023. Neural grasp distance fields for robot manipulation, in: 2023 IEEE International Conference on Robotics and Automation (ICRA), IEEE. pp. 1814–1821.
- Yen-Chen, L., Florence, P., Barron, J.T., Rodriguez, A., Isola, P., Lin, T.Y., 2021. inerf: Inverting neural radiance fields for pose estimation, in: 2021 IEEE/RSJ International Conference on Intelligent Robots and Systems (IROS), IEEE. pp. 1323–1330.
- Zeng, A., Florence, P., Tompson, J., Welker, S., Chien, J., Attarian, M., Armstrong, T., Krasin, I., Duong, D., Sindhwani, V., et al., 2020. Transporter networks: Rearranging the visual world for robotic manipulation. [arXiv preprint arXiv:2010.14406](#) .
- Zhou, Y., Barnes, C., Lu, J., Yang, J., Li, H., 2019. On the continuity of rotation representations in neural networks, in: Proceedings of the IEEE/CVF Conference on Computer Vision and Pattern Recognition, pp. 5745–5753.